Monthly Notices
of the
ROYAL ASTRONOMICAL SOCIETY

Mon. Not. R. Astron. Soc. **401,** 2561–2571 (2010) doi:10.1111/j.1365-2966.2009.15834.x

Determining the escape fraction of ionizing photons during reionization with the GRB-derived star formation rate

J. S. B. Wyithe,[1⋆] A. M. Hopkins,[2] M. D. Kistler,[3,4] H. Yüksel[5] and J. F. Beacom[3,4,6]

[1]*School of Physics, University of Melbourne, Parkville, Victoria, Australia*
[2]*Anglo-Australian Observatory, PO Box 296, Epping, NSW 1710, Australia*
[3]*Center for Cosmology and Astro-Particle Physics, The Ohio State University, 191 W. Woodruff Ave., Columbus, OH 43210, USA*
[4]*Department of Physics, The Ohio State University, 191 W. Woodruff Ave., Columbus, OH 43210, USA*
[5]*Bartol Research Institute and Department of Physics and Astronomy, University of Delaware, Newark, DE 19716, USA*
[6]*Department of Astronomy, The Ohio State University, 140 W. 18th Ave., Columbus, OH 43210, USA*

Accepted 2009 October 5. Received 2009 October 5; in original form 2009 August 3

ABSTRACT

The fraction of ionizing photons that escape their host galaxies and so are able to ionize hydrogen in the inter-galactic medium (IGM) is a critical parameter in the analyses of the reionization era and early galaxy formation. Studies of the reionization history normally suffer from a degeneracy between the unknown values for the efficiency with which high-redshift galaxies turn mass into stars and the escape fraction of ionizing photons. Recent gamma-ray burst (GRB) measurements of the star formation rate density during reionization provide the first opportunity to break this degeneracy. We confront a semi-analytic model for reionization with the GRB-derived star formation rate, as well as observations of the Lyα forest and the CMB. Assuming that UV photons produced in star-forming galaxies dominate the reionization process, we show that the escape fraction of ionizing photons from high-redshift galaxies is $\sim$5 per cent [$\log f_{\rm esc} = -1.35 \pm 0.15$ (68 per cent)] for our fiducial model. This relatively small value of escape fraction follows from the slow evolution in the star formation rate density at $z \gtrsim 4$ implied by the number counts of high-redshift GRBs. Our derived value is reasonably stable against uncertainties in the modelling, including the implementation of radiative feedback, the possibility of an evolving escape fraction and the unknown shape of the IMF, which in sum contribute $\sim$0.2 dex of additional systematic uncertainty on the value of escape fraction.

Key words: galaxies: high-redshift – intergalactic medium – diffuse radiation – cosmology: theory – large scale structure of Universe.

Downloaded from http://mnras.oxfordjournals.org/ by guest on February 28, 2013

1 INTRODUCTION

Star-bursting galaxies and quasars have been the leading candidates for the sources of the UV radiation required to reionize the hydrogen gas in the inter-galactic medium (IGM) (e.g. Barkana & Loeb 2001). The quasar population is observed to decline quickly at $z \gtrsim 2.5$, and so it is believed that it was galaxies that contributed the bulk of UV photons that drove reionization (Madau, Haardt & Rees 1999; Fan et al. 2002; Srbinovsky & Wyithe 2007; Bolton & Haehnelt 2007). However, it has been difficult to make a positive case for galaxies as opposed to favouring them by disfavouring the case for quasars. The contribution of galaxies to the UV radiation field is dependent on the star formation rate and initial stellar mass function, but is also limited by the fraction of ionizing photons that escape their host galaxies. If the escape fraction is small, then star formation had to be very efficient at high redshift in order to reionize the Universe. The escape fraction is therefore a critical parameter in studies of the connection between high-redshift galaxy formation and reionization.

Attempts to determine the escape fraction have been dominated by direct observations of relatively low redshift galaxies, and by numerical simulation. The escape fraction of ionizing photons from the Milky Way galaxy can be reliably measured by modelling the observed emission measures and kinematics of the Magellanic stream in the presence of photoionization due to hot, young stars in the Galactic disc, yielding a value of $\sim$6 per cent (Bland-Hawthorn & Maloney 1999). In extra-galactic cases, direct measurements of the escape fraction ($f_{\rm esc}$) are complicated by the fact that the intrinsic number of ionizing photons produced by a specific galaxy is unknown. A commonly adopted strategy to circumvent this limitation is to compare the flux observed at the Lyman limit to the

⋆E-mail: swyithe@unimelb.edu.au

© 2009 The Authors. Journal compilation © 2009 RAS

observed flux at a frequency where the intrinsic emissivity can be inferred (Leitherer et al. 1995; Deharveng et al. 2001; Steidel, Pettini & Adelberger 2001; Siana et al. 2007; Cowie, Barger & Trouille 2009; Iwata et al. 2009). The escape fraction at the Lyman limit can then be derived using a model description of the star formation history (Leitherer et al. 1995; Steidel et al. 2001; Siana et al. 2007). However, the results are currently uncertain, with no confident detections at $0 < z < 1$, and only some detections at $z > 3$. At redshifts $z \sim 1$–3, observations have suggested a broader range of values for $f_{\rm esc}$, from a few per cent to ∼20 per cent (Steidel, Pettini & Adelberger 2001; Fernández-Soto, Lanzetta & Chen 2003; Shapley et al. 2006; Siana et al. 2007). Inoue, Iwata & Deharveng (2006) have examined the evolution of the escape fraction in the redshift range $z = 0$–6 using both direct observations of the escape fraction and values that they derive from the measurements of the ionizing background. They find that the escape fraction evolves from $f_{\rm esc} \sim 1$–10 per cent, increasing towards high redshift. More recently, Fynbo et al. (2009) (see also Chen, Prochaska & Gnedin 2007) have used spectroscopic observations of individual gamma-ray burst (GRB) afterglows at $z > 2$ to place a 95 per cent confidence upper limit of 7.5 per cent on the escape fraction for ionizing photons on the GRB sight lines, although they note a possible bias towards small values of $f_{\rm esc}$.

Theoretical modelling has concentrated on the absorption of ionizing photons as they propagate through the inter-stellar medium towards the IGM. Here, also the results are not yet conclusive. For example, Wood & Loeb (2000) found $f_{\rm esc} \lesssim 1$ per cent at $z \sim 10$ suggesting that the escape fraction decreases towards high redshift due to the increased density of galactic discs. More recently, Razoumov & Sommer-Larsen (2006) used galaxy formation simulations incorporating high-resolution 3D radiative transfer to show that the escape fraction evolves from $f_{\rm esc} \sim 1$–2 per cent at $z = 2.39$ to $f_{\rm esc} \sim 6$–10 per cent at $z = 3.6$. In agreement with Fujita et al. (2003), Razoumov & Sommer-Larsen (2006) (see also Yajima et al. 2009) find that increased supernova feedback at higher redshift expels gas from the vicinity of star-bursting regions, creating tunnels in the galaxy through which ionizing photons can escape into the IGM. They also find that star formation may occur at slightly lower densities at higher redshift, which further contributes to the increased $f_{\rm esc}$ towards higher redshift.

Numerical simulations (Gnedin, Kravtsov & Chen 2008) have been presented that predict a value for $f_{\rm esc}$ between 1 and 3 per cent, for haloes of mass $M \gtrsim 5 \times 10^{10}\,{\rm M}_{\odot}$, over the redshift range $3 < z < 9$. This very low efficiency of reionization would have profound effects on the reionization history. In addition to a small escape fraction in massive galaxies, Gnedin et al. (2008) further predict that haloes with $M \lesssim 5 \times 10^{10}\,{\rm M}_{\odot}$ have an escape fraction that is negligibly small. However, more recently Wise & Cen (2009) have used a large suite of simulations to show that the time-averaged escape fraction for dwarf galaxies is expected to be large (>25 per cent). Since dwarf galaxies are thought to dominate the ionizing flux, resolution of this issue is of primary importance for studies of reionization.

A less direct avenue to determining the escape fraction is through modelling of the ionizing background at the end of reionization. Models of the reionization of hydrogen and the subsequent Lyα forest are subject to a degeneracy between the star formation efficiency of gas accreted into galaxies and the fraction of ionizing photons that escape the dense gaseous environment of the galaxy to ionize the IGM. In order to break this degeneracy, the true cosmic star formation rate must be known. For example, the escape fraction has been estimated at high redshifts by combining the ionization rate in the IGM with an estimate of the star formation rate obtained from measurements of the galaxy luminosity function (e.g. Bolton & Haehnelt 2007; Srbinovsky & Wyithe 2008; Faucher-Giguère et al. 2008). Assuming that the mean-free path is accurately estimated, the escape fraction follows from comparison of the total number of photons produced with the number that are ionizing the IGM. The primary drawback of this technique is that the observed luminosity functions are subject to uncertain corrections for extinction in galaxies, as well as a flux limit. The latter fact means that an extrapolation to lower galaxy luminosities must be performed in order to obtain a total star formation rate.

GRBs are now beginning to probe the star formation rate density in the era during which the Universe is thought to have become reionized (Salvaterra et al. 2009; Tanvir et al. 2009). In this paper, we employ the recent determination of the star formation rate density (Kistler et al. 2009) out to $z \sim 8.5$ based on a compilation of high-redshift GRBs. As described below, this measurement of the cosmic star formation rate with GRBs is not subject to the usual large corrections required for extinction and unseen faint galaxies. By modelling the reionization of hydrogen, we determine the star formation efficiency and escape fraction that is required to simultaneously reproduce the optical depth to electron scattering of CMB photons, the star formation rate density during the reionization era and the ionizing background at the end of reionization. Inclusion of the star formation rate density as a constraint allows the star formation efficiency and escape fraction to be separately determined.

Our analysis is similar to that of Choudhury & Ferrara (2005, 2006), who modelled the reionization history and compared model predictions to a range of observables, including the star formation rate, the ionization rate from the Lyα forest and the optical depth to electron scattering of CMB photons, as well as the evolution of Lyman limit systems and the temperature of the IGM among others. However, here we limit our attention to the first three of these observables that most directly relate to the determination of the escape fraction, and which can be most reliably predicted by an analytic model. Most importantly, we make use of the recent determination of star formation rate density from GRBs, which for the first time provide a measurement of the total star formation deep into the reionization era. We also quantify the statistical and systematic uncertainties on the model parameters.

The paper is organized as follows. In Section 2, we discuss the determination of star formation rate density from high-redshift GRBs, and review a simple estimate of the ionizing photon budget for reionization. We then describe other observational constraints (Section 3), as well as our semi-analytic model for reionization (Section 4). The resulting limits on the possible values of model parameters are presented in Sections 5 and 6. We conclude with a summary of our results for the escape fraction in Section 7. In our numerical examples, we adopt the standard set of cosmological parameters (Komatsu et al. 2009), with values of $\Omega_{\rm b} = 0.04$, $\Omega_{\rm m} = 0.24$ and $\Omega_{\Lambda} = 0.76$ for the matter, baryon and dark energy fractional density, respectively, $h = 0.73$, for the dimensionless Hubble constant, and $\sigma_8 = 0.81$ for the variance of the linear density field within regions of radius $8\,h^{-1}$Mpc.

2 A GRB DETERMINATION OF THE STAR FORMATION RATE DENSITY AT HIGH REDSHIFT

Kistler et al. (2009) (following Yüksel et al. 2008) have used the counts of GRBs at high redshift to infer the star formation rate

Downloaded from http://mnras.oxfordjournals.org/ by guest on February 28, 2013

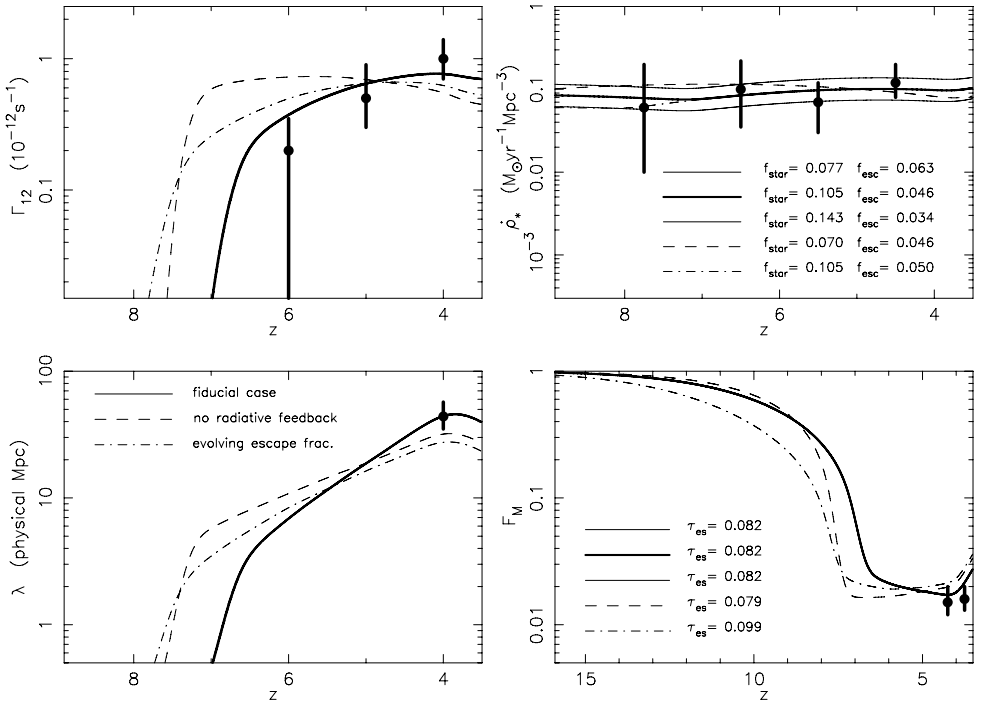

Figure 1. Models for the reionization of the IGM and the subsequent post-overlap evolution of the ionizing radiation field. In each panel, five cases are shown, with line styles corresponding to the cases in Figs 2 and 3. The three solid lines shown correspond to the best-fitting (thick line) and 1σ deviations for the fiducial case with $T_{\rm min} = 10^4$ K and $T_{\rm ion} = 10^5$ K (note that these three cases for the fiducial model overlap in some of the panels). The dashed line shows a case with $T_{\rm min} = T_{\rm ion} = 10^4$ K. The dot–dashed line shows a case with $T_{\rm min} = 10^4$ K and $T_{\rm ion} = 10^5$ K, but $f_{\rm esc} \propto (1 + z)$. The models are labelled by the values of $f_\star$, $f_{\rm esc}$ and $\tau_{\rm es}$. A value of $\Delta_{\rm c} = 10$ was chosen for the critical overdensity prior to the overlap epoch. The histories shown correspond to best-fitting models based on constraints from Γ_{12} and $\dot{\rho}_\star$ at $z > 4$, and also $\tau_{\rm es}$. Upper-left panel: the ionization rate as a function of redshift. The observational points are from Bolton & Haehnelt (2007). Upper-right panel: the star formation rate density as a function of redshift. The data points are from Kistler et al. (2009). Lower-left panel: the mean-free-path for ionizing photons. The data point is based on Storrie-Lombardi et al. (1994). Lower-right panel: the volume and mass averaged fractions of neutral gas in the universe. The observational points for the mass-fractions are from the damped Lyα measurements of Prochaska et al. (2005).

density out to $z \sim 8.5$. Inspection of their fig. 4 (see also Fig. 1 of this paper) suggests that the star formation rate density is as large as or could even be higher at $z \sim 8$ than at $z \sim 4$–6, implying that the ionizing photon emissivity is not falling as observations move into the reionization era. This inference requires an assumption for the initial mass function (IMF). However, since both ionizing photons and GRBs are produced by massive stars, estimates of the ionizing photon emissivity from the GRB rate should be fairly robust against uncertainties in the IMF (this point is taken up quantitatively in Section 5.5).

Kistler et al. (2009) argued that we have observed enough star formation via high-redshift GRBs at $z \gtrsim 6$ to reionize the universe, even with a relatively small value of $f_{\rm esc}$. In this paper, we extend their simple estimates. Specifically, we constrain the possible values of escape fraction by modelling the reionization history and comparing with the observed star formation rate density as traced by high-redshift GRBs, the ionization rate as traced by the Lyα forest at $z < 6$ and the optical depth to the Thomson scattering of CMB photons. The GRB-derived star formation rate density values that were presented in Kistler et al. (2009) are special in three ways with respect to breaking the degeneracy between escape fraction and star formation efficiency during the reionization era.

First, the star formation rate density is based on number counts of GRBs which yields the absolute death/birth rate of massive stars. These number counts are independent of obscuration and absorption effects that limit the utility of UV emission as a direct indicator of star formation rate. The utility of counting events marking the death of individual stars in order to get the star formation rate density has also been argued by Lien & Fields (2009) in the context of supernovae at lower redshift.

Secondly, GRBs are thought to sample the full luminosity range of galaxies, so that no correction for luminosity function is required. In conventional studies of the star formation rate, one attempts to correct for this problem, but there are uncertainties (e.g. Hopkins & Beacom 2006). The GRB results from Kistler et al. (2009) confirm the two large corrections (for obscuration and luminosity function) applied to the raw results of Bouwens et al. (2008). It could therefore be argued that this agreement implies the combined corrections are approximately correct, suggesting the absence of any deep misunderstandings about the properties of high-redshift galaxies. Conversely, if the luminosity function correction applied to the Bouwens et al. (2008) data by Kistler et al. (2009) is appropriate, then most of the total star formation during the reionization era was within small galaxies. With regard to this point, it is important to note that in more local samples, most GRB hosts are found to be low-mass galaxies (Fruchter et al. 2006; Stanek et al. 2006). This implies that GRBs are an efficient probe of low-mass galaxy formation, and is in contrast to studies of the UV luminosity function at $z > 6$ that currently probe only the most massive galaxies. Since low-mass galaxies seem to be dominant during the reionization era, we therefore argue that GRBs provide the most important constraints on the star formation rate density during reionization, and utilize the star formation values from Kistler et al. (2009) in our parameter constraints.

Downloaded from http://mnras.oxfordjournals.org/ by guest on February 28, 2013

The third fundamental advantage of using GRBs to determine the star formation rate density is that the data now go deep into the reionization era. This makes them a rather direct probe of the star formation responsible for reionization.

2.1 Summary of star formation rate density from high-z GRBs

As discussed above, Kistler et al. (2009) have determined the star formation rate density deep into the reionization era based on the occurrence of GRBs at $z > 6$. We use as constraints the determination of star formation rate density based on GRBs between $4 \lesssim z \lesssim 8.5$ from Kistler et al. (2009). In units of solar masses per year per cubic Mpc, the values[1] used are $\dot{\rho}_{\star,\rm obs} = 0.05^{+0.14}_{-0.04}$ at $z = 7.75 \pm 0.75$, $\dot{\rho}_{\star,\rm obs} = 0.09^{+0.12}_{-0.06}$ at $z = 6.5 \pm 0.5$, $\dot{\rho}_{\star,\rm obs} = 0.07^{+0.05}_{-0.04}$ at $z = 5.5 \pm 0.5$ and $\dot{\rho}_{\star,\rm obs} = 0.12^{+0.07}_{-0.05}$ at $z = 4.5 \pm 0.5$. When combined with the fact that CMB constraints (Komatsu et al. 2009) place most of the reionization at $z \sim 10$, this implies that we now have multiple constraints probing epochs during the reionization era. These data are shown in the upper-right panel of Fig. 1.

2.2 Uncertainties in estimates of high-redshift star formation

The utility of using the GRB rate to determine the star formation rate follows from the proportionality between these two closely related quantities. There is therefore a component of uncertainty in the estimation of the star formation rate originating from the Poisson noise in the number of GRBs observed (Kistler et al. 2008, 2009). In addition to this Poisson noise, it is apparent from equation (4) of Kistler et al. (2009) that there are three other components of uncertainty. First, there is also Poisson error in the number of GRBs in the redshift range $1 < z < 4$ that is used to determine the normalization of the relation between GRB and star formation rate. However, in each high-redshift range considered by Kistler et al. (2009), the number used for normalization is much larger than the number used to infer the star formation rate at high redshift. For example, in the highest redshift bin $7 < z < 8.5$, there is one GRB, which is compared with the nine GRBs of comparable luminosity at $1 < z < 4$. Poisson uncertainty in the latter is therefore negligible[2] with respect to the calculation of uncertainty in the inferred star formation rate (Gehrels 1986). Secondly, there is measurement error due the observed star formation rate in the redshift range $1 < z < 4$. Hopkins & Beacom (2006) list a compilation of ∼16 observations in the range $1 < z < 4$, each with an error bar of ∼50 per cent. The statistical uncertainty in the integrated star formation rate density at $1 < z < 4$ is therefore smaller than ∼50 per cent, though common errors between the data points mean that these points cannot be treated as independent. However, the uncertainty in the star formation rate is much smaller than the Poisson error in the small numbers of GRBs at $z > 4$. Thirdly, there is evolution in the ratio between the star formation and GRB rates that can be described by a factor proportional to $(1 + z)^{\alpha}$ (Kistler et al. 2008). Kistler et al. (2009) show that $\alpha \sim 1.2$ best describes the relative evolution of the star formation and GRB rates in the range $(1 < z < 4)$, with a 1σ uncertainty of $\Delta\alpha \sim 0.6$. This range corresponds to a ∼20 per cent uncertainty in the inferred star formation rate at $z \sim 7.75$.

Thus, the uncertainty in estimates of the high-redshift star formation rate is dominated by the small numbers of high-redshift GRBs (Kistler et al. 2009), and the corresponding Poisson error is therefore adopted for the estimate of uncertainty in the quoted values of star formation rate density. As a result, the addition of more high-redshift GRBs in the future will aid our understanding of the reionization era by lowering the statistical errors on estimation of the star formation rate density.

3 ADDITIONAL OBSERVATIONAL CONSTRAINTS

In this section, we summarize two additional pieces of data that constrain the possible scenarios in addition to the GRB-derived star formation rate density.

3.1 Thomson scattering optical depth for CMB photons

The measured optical depth to Thomson scattering of CMB photons measures the column density of ionized hydrogen between the observer and the surface of last scattering. The latest observed value of $\tau_{\rm es} = 0.084 \pm 0.016$ implies that reionization did not occur significantly beyond $z \sim 10$ (Komatsu et al. 2009). When computing $\tau_{\rm es}$ from the reionization history we assume that the filling factor of singly ionized helium equals the ionized fraction of hydrogen, and that helium becomes doubly ionized at $z = 3$ (Wyithe & Loeb 2003).

3.2 Ionization rate from the Lyα forest

Observations of the Gunn–Peterson optical depth in the high-redshift Lyα forest imply a very highly ionized IGM at $z \lesssim 6$, suggesting that reionization was complete by that time. The intensity of the ionizing background implied by the effective Lyα optical depth is sensitive to the details of the distribution of gas densities and temperatures, but can be reliably modelled via numerical simulation (e.g. Bolton & Haehnelt 2007). We take values for the ionization rate at $4 \lesssim z \lesssim 6$ from the simulations of Bolton & Haehnelt (2007), based on the observations of Fan et al. (2006). In units of 10^{-12} s^{-1} the values used are $\Gamma_{\rm obs} = 0.2^{+0.15}_{-0.2}$ at $z = 6$, $\Gamma_{\rm obs} = 0.5^{+0.4}_{-0.2}$ at $z = 5$, $\Gamma_{\rm obs} = 1^{+0.4}_{-0.3}$ at $z = 4$, respectively. These data are shown in the upper-left panel of Fig. 1.

4 SEMI-ANALYTIC MODEL FOR REIONIZATION

In this section, we summarize the semi-analytic model used to calculate the reionization history of the IGM. The basis of this model is the differential between ionization and recombination rates for hydrogen in an inhomogeneous IGM. Miralda-Escudé, Haehnelt & Rees (2000) presented a model that allows the calculation of an effective recombination rate in an inhomogeneous universe by assuming a maximum overdensity ($\Delta_{\rm c}$) penetrated by ionizing photons within H II regions. The model assumes that reionization progresses rapidly through islands of lower density prior to the overlap of individual cosmological ionized regions. Following the overlap epoch, the remaining regions of high density are gradually ionized. It is therefore hypothesized that at any time, regions with gas below some critical overdensity $\Delta_{\rm i} \equiv \rho_i/\langle\rho\rangle$ are highly ionized while

[1] The cosmology used in this paper is slightly different from Kistler et al. (2009). This difference propagates through the estimate of star formation rate via the calculated value of comoving volume. However, we have not modified the published values as the numerical value corresponding to the volume change is very much smaller than the statistical uncertainties.

[2] For example, the addition in quadrature of a 20 per cent relative uncertainty to a relative uncertainty that is of the order of unity results in only a 2 per cent increase in the relative error.

Downloaded from http://mnras.oxfordjournals.org/ by guest on February 28, 2013

regions of higher density are not. The fraction of mass in regions with overdensity below Δ_i is found from the integral

$$F_M(\Delta_i) = \int_0^{\Delta_i} d\Delta P_V(\Delta)\Delta, \quad (1)$$

where $P_V(\Delta)$ is the volume-weighted probability distribution for Δ. Miralda-Escudé et al. (2000) quote a fitting function that provides a good fit to the volume-weighted probability distribution for the baryon density in cosmological hydrodynamical simulations. In what follows, we draw primarily from the prescription of Miralda-Escudé et al. (2000) and refer the reader to the original paper for a detailed discussion of its motivations and assumptions. Wyithe & Loeb (2003) employed this prescription within a semi-analytic model of reionization. This model was extended by Srbinovsky & Wyithe (2007) and by Wyithe, Bolton & Haehnelt (2008). We refer the reader to those papers for a full description.

The quantity Q_i is defined to be the volume filling factor within which all matter at densities below Δ_i has been ionized. The reionization history is quantified by the evolution of Q_i that evolves according to the rate equation

$$\frac{dQ_i}{dz} = \frac{1}{n_0 F_M(\Delta_i)} \frac{dn_\gamma}{dz} - \left[\alpha_B (1+z)^3 R(\Delta_i) n_0 \frac{dt}{dz} + \frac{dF_M(\Delta_i)}{dz}\right] \frac{Q_i}{F_M(\Delta_i)}, \quad (2)$$

where α_B is the case B recombination coefficient, n_0 is the comoving density of hydrogen in the mean IGM, and $R(\Delta_i)$ is the effective clumping factor of the IGM. The evolution is driven by the rate of emission of ionizing photons per comoving volume dn_γ/dz. Within this formalism, the epoch of overlap is precisely defined as the time when Q_i reaches unity. Prior to the overlap epoch we must solve for both Q_i and F_M (or equivalently Δ_i). The relative growth of these depends on the luminosity function and spatial distribution of the sources. In this regime, we assume Δ_i to be constant with redshift before the overlap epoch and compute results for models with values of $\Delta_i \equiv \Delta_c = 10$. Different values of Δ_c are not found to quantitatively affect our results for values in the range $5 < \Delta_c < 20$ (Wyithe et al. 2008).

Following overlap, we may describe the post-overlap evolution of the IGM by computing the evolution of the ionized mass fraction according to the equation:

$$\frac{dF_M(\Delta_i)}{dz} = \frac{1}{n_0}\frac{dn_\gamma}{dz} - \alpha_B (1+z)^3 R(\Delta_i) n_0 \frac{dt}{dz}. \quad (3)$$

Note that this follows directly from equation (2) with $Q_i = 1$, and that in this post-overlap regime the value of Δ_i is the dependent variable describing the ionization state of the IGM (whereas prior to overlap $\Delta_i = \Delta_c$). Equation (3) is integrated to obtain F_M (or equivalently Δ_i) as a function of redshift.

The emission rate of ionizing photons per comoving volume that is required to compute the reionization history can be written as

$$\frac{dn_\gamma}{dz} = N_\gamma f_{esc} \frac{\dot{\rho}_\star}{m_p} \frac{dt}{dz}, \quad (4)$$

where N_γ is the number of ionizing photons produced per baryon incorporated into stars, and $\dot{\rho}_\star$ is the star formation rate per unit volume. As described in the Introduction, only a fraction of ionizing photons produced by stars enter the IGM. Therefore, an additional factor of f_{esc} (the escape fraction) must be included when computing the ionizing emissivity of galaxies. There are expected to be large fluctuations in escape fraction with time and with viewing angle for individual galaxies. The escape fraction could also depend on galaxy mass (Gnedin et al. 2008; Wise & Cen 2009). However, what is important for studies of the overall photon budget during reionization is the total cosmic ionizing flux, rather than the ionizing flux near a particular galaxy (although of course the latter could affect statistics of Lyα absorption or 21cm emission from the IGM). In our model, we therefore assume a single value for f_{esc}, which should be interpreted as a stellar mass averaged value over star-forming galaxies.

The star formation rate per unit volume is computed based on the collapsed fraction $[(dF_{col}(M))/dt]$ obtained from the Press & Schechter (1974) model in haloes above the minimum halo mass (M) for star formation, together with an assumed star formation efficiency ($f_\star$)

$$\dot{\rho}_\star = f_\star \rho_c \Omega_B \left[(1-Q_i)\frac{dF_{col}(M_{min})}{dt} + Q_i \frac{dF_{col}(M_{ion})}{dt}\right], \quad (5)$$

where ρ_c is the critical density and the collapsed fraction includes separate components from ionized and neutral regions of IGM. In a cold neutral IGM beyond the redshift of reionization, the collapsed fraction should be computed for haloes of sufficient mass to initiate star formation. The critical virial temperature is set by the temperature ($T_{min} \sim 10^4$ K) above which efficient atomic hydrogen cooling promotes star formation. Following the reionization of a region, the Jeans mass in the heated IGM limits accretion to haloes above $T_{ion} \sim 10^5$ K (Efstathiou 1992; Thoul & Weinberg 1996; Dijkstra et al. 2004). Thus, once N_γ, T_{min} and T_{ion} are specified, the reionization model has two free parameters, $f_\star$ and f_{esc}.

In order to estimate the ionizing background following the end of reionization, our approach is to compute a reionization history given a particular value of Δ_c, combined with assumed values for the efficiency of star formation and the fraction of ionizing photons that escape from galaxies. With this history in place, we then compute the evolution of the background radiation field due to these same sources. After the overlap epoch, ionizing photons will experience attenuation due to residual overdense pockets of H I gas. We use the description of Miralda-Escudé et al. (2000) to estimate the ionizing photon mean-free path [with a reduction of the constant of proportionality by a factor of 2 following the discussion of Oh & Furlanetto (2005)], and subsequently derive the attenuation of ionizing photons. We then compute the flux at the Lyman-limit in the IGM due to sources immediate to each epoch, in addition to redshifted contributions from earlier epochs.

4.1 Stellar production of ionizing photons

In our modelling, we assume spectral energy distributions (SED) of Population II star-forming galaxies using the model presented in Leitherer et al. (1999). We assume stars of 0.05 solar metallicity (the effect of metallicity is discussed in Section 5.5), and calculate the number (N_γ) of ionizing photons above the ionization threshold for hydrogen. This number is calculated for continuous star formation, and the low metallicity is reasonable at high redshift. The mass functions each have lower and upper limits of 0.1 $M_\odot$ and 120 $M_\odot$, respectively. Taking the functional form $dn/dM \propto M^{-\alpha}$, our fiducial model has a Salpeter IMF with $\alpha = 2.35$. With these choices we find $N_\gamma = 4648$ in our fiducial model.

In later sections, we also employ three additional IMF to gauge the systematic uncertainty. These are summarized in Table 1, along with the fiducial Salpeter case. As in our fiducial case, we assume stars of 0.05 solar metallicity, and present the number of ionizing photons above the ionization threshold for hydrogen. This number is again calculated with mass functions that have lower and upper

Downloaded from http://mnras.oxfordjournals.org/ by guest on February 28, 2013

Table 1. Summary of IMFs used in this work. Values of N_γ have units of photons per baryon.

IMF	$\alpha_{\rm low}$	α	$\dot{\rho}_\star/\dot{\rho}_{\rm sal}$	N_γ	$N_\gamma/N_{\rm sal}$	$f_{\rm IMF}$
Salpeter	-	2.35	1	4648	1	1.00
Salpeter A	1.5	2.35	0.77	6034	1.30	1.00
BG03	1.5	2.15	0.50	11139	2.39	1.20
Top-heavy	-	1.95	0.37	17553	2.75	1.39

limits of 0.1 $M_\odot$ and 120 $M_\odot$, respectively. We consider two cases with turnover in the mass function below 0.5 $M_\odot$ (with an index in that mass range of $\alpha = 1.5$). These cases have high mass indexes of $\alpha = 2.35$ (labelled Salpeter A) and $\alpha = 2.15$ (Baldry & Glazebrook 2003, labelled BG), respectively. The Salpeter A and BG IMFs were identified by Hopkins & Beacom (2006) as providing reasonable bounds on the normalization of the cosmic star formation history. We also consider the case of a top-heavy mass function having a single index of $\alpha = 1.95$ across the entire mass range. The values for N_γ are listed in Table 1, demonstrating that more top-heavy mass functions produce a larger fraction of their energy as photons above the ionization threshold. The ratio relative to the value $N_{\rm sal} = 4648$ for a Salpeter mass function is also presented in the second last column for ease of comparison.

5 CONSTRAINTS ON MODELS OF THE REIONIZATION HISTORY

In this section, we confront our model for reionization with the three pieces of data described in earlier sections in order to constrain the possible scenarios.

5.1 Parameter constraints

From the above observations, we constrain the possible parametrizations of our model for the reionization history. In addition to hypothesized parameters Δ_c, $T_{\rm min}$ and $T_{\rm ion}$, our reionization model has two free parameters, $f_\star$ and $f_{\rm esc}$, for combinations of which we compute the reionization history, and calculate the χ^2 of the model as

$$\chi^2(f_\star, f_{\rm esc}) = \sum_{i=0}^{N_{\Gamma,\rm obs}} \left[\frac{\log\Gamma(f_\star, f_{\rm esc}, z_i) - \log\Gamma_{\rm obs}(z_i)}{\sigma_\Gamma(z_i)}\right]^2 + \sum_{i=0}^{N_{\dot{\rho}_\star,\rm obs}} \left[\frac{\log\dot{\rho}_\star(f_\star, f_{\rm esc}, z_i) - \log\dot{\rho}_{\star,\rm obs}(z_i)}{\sigma_\rho(z_i)}\right]^2 + \left[\frac{\tau_{\rm es}(f_\star, f_{\rm esc}) - \tau_{\rm es,obs}}{\sigma_\tau}\right]^2. \quad (6)$$

Here, $\Gamma_{\rm obs}(z_i)$ and $\dot{\rho}_\star(z_i)$ are the observed ionization rates and star formation rate densities measured at a number of redshifts (z_i), with uncertainty $\sigma_\Gamma(z_i)$ and $\sigma_\rho(z_i)$ in dex, and $\tau_{\rm es,obs}$ is the observed optical depth to the Thomson scattering of CMB photons with uncertainty σ_τ (in dex). We note that the error bars on the observational estimates are not symmetric. We deal with this approximately by calculating the contribution to χ^2 using the error bar either above or below the best-fitting value, according to which reflects the model prediction.

5.2 Constraints on the escape fraction in the fiducial model

In the upper-left panel of Fig. 2, we present constraints on the parameters $f_\star$ and $f_{\rm esc}$ assuming our fiducial model with $T_{\rm min} = 10^4$ K, and $T_{\rm ion} = 10^5$ K. As a first illustration, we have included the available constraints on $\tau_{\rm es}$ as well as on Γ, but have neglected $\dot{\rho}_\star$ in order to highlight the importance of its inclusion with the latter examples. The allowed region in this case is shown by the grey shading. The ionizing background radiation, and the duration of the reionization epoch as measured by $\tau_{\rm es}$, constrain the combination $f_{\rm star}\, f_{\rm esc}$ (Barkana & Loeb 2001; Srbinovsky & Wyithe 2008). This degeneracy can be clearly seen in Fig. 2. The dark solid contours that are overplotted in the upper-left panel of Fig. 2 show the corresponding constraints following the addition of the measurements of $\dot{\rho}_\star$ from $z > 4$. The star formation rate breaks this degeneracy, since the star formation rate density predicted by the model is not directly dependent[3] on $f_{\rm esc}$. As a result, $f_\star$ and $f_{\rm esc}$ can be separately constrained yielding values of $0.077 \lesssim f_\star \lesssim 0.143$ and $0.030 \lesssim f_{\rm esc} \lesssim 0.070$ for the fiducial model. The best-fitting model has the parameter combination $(f_\star,\ f_{\rm esc}) = (0.105, 0.046)$, with a value of $\chi^2_{\rm min} = 2.3$. This value is total rather than per degree-of-freedom, and is surprisingly low given a two-parameter fit and eight data points. However, we note that the values for three additional free parameters have been chosen in this model ($T_{\rm min}$, $T_{\rm ion}$ and Δ_c). Different values for these are assumed below, leading to larger χ^2 values.

In Fig. 1, we show models (solid lines) corresponding to the best fit, $(f_\star,\ f_{\rm esc}) = (0.105, 0.046)$, as well as models near the edge of the 1σ contour, $(f_\star,\ f_{\rm esc}) = (0.077, 0.063)$ and $(f_\star,\ f_{\rm esc}) = (0.143, 0.034)$. The locations of these models in the $f_\star$–$f_{\rm esc}$ plane are shown by dots in Fig. 2. In the upper-left and upper-right panels of Fig. 1, we show the evolution of the ionization rate and star formation rate density, respectively. In the lower-left and lower-right panels, we show the evolution of the ionizing photon mean-free path and mass-averaged neutral fraction that are also predicted by the model. Note that the quantities other than star formation rate density are degenerate for these parameter combinations. The data points for mean-free path are based on Storrie-Lombardi et al. (1994). The observational points for the mass fractions are from the damped Lyα measurements of Prochaska, Herbert-Fort & Wolfe (2005), and therefore represent lower limits on the total H I content of the IGM. In both cases, the curves show excellent agreement with these quantities, even though they were not included as part of the parameter fit. The values of $\tau_{\rm es}$ for these models are listed in the lower-right panel. The universe is predicted to be 50 per cent ionized at $z \sim 9.5$.

We note that the observed mean-free path is found from the number density of Ly-limit systems and is independent of the Lyα forest absorption derived quantities of ionization rate and volume-averaged neutral fraction, as well as being independent of the H I mass–density measurements. Our simple model therefore simultaneously reproduces the evolution of four independent measured quantities, as well as the optical depth to electron scattering of CMB photons.

Despite this success, the accuracy of estimates for the ionization rates predicted by the model could be questioned, primarily because of the sensitivity of the calculation of the mean-free path to the probability distribution for Δ. To test the sensitivity of our

[3] There is an indirect dependence of star formation rate density on $f_{\rm esc}$ because the star formation rate in equation (5) depends on the fraction of universe ionized at a particular time.

Downloaded from http://mnras.oxfordjournals.org/ by guest on February 28, 2013

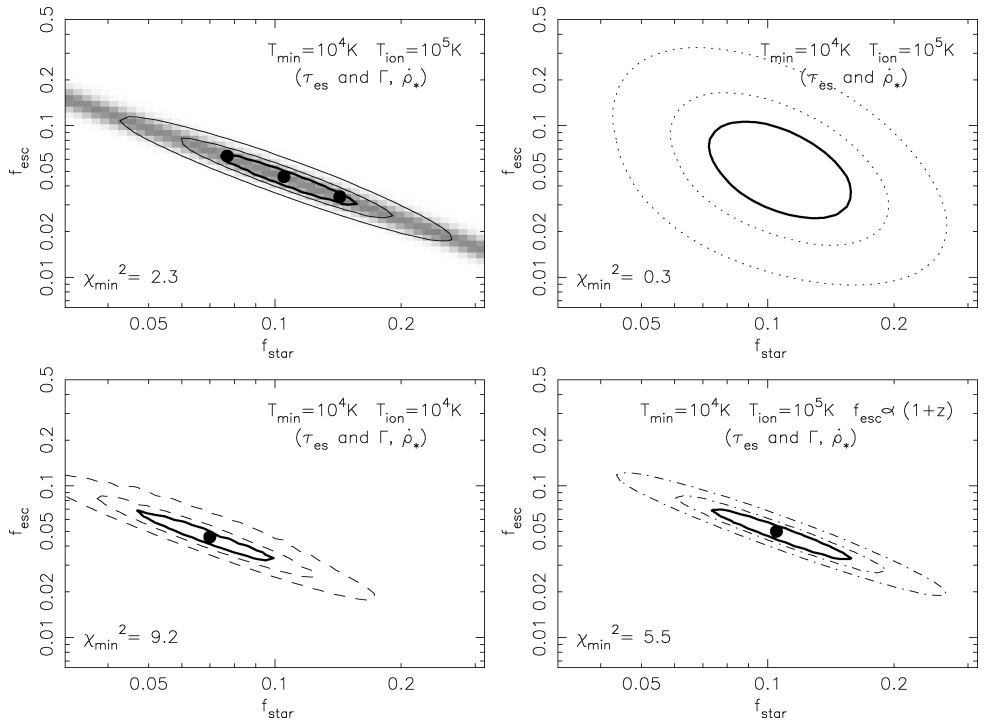

Figure 2. Joint constraints on the parameters $f_\star$ and $f_{\rm esc}$ based on observations of the star formation rate density $\dot{\rho}_\star$, the ionization rate Γ_{12} and the optical depth to the Thompson scattering of CMB photons $\tau_{\rm es}$. Upper left: the fiducial model with $T_{\rm min} = 10^4$ K and $T_{\rm ion} = 10^5$ K. Constraints on Γ_{12} and $\dot{\rho}_\star$ are used at $z > 4$. Also shown for comparison are the constraints on this model if measurements of $\dot{\rho}_\star$ are ignored, which reveals how the GRB star formation data break the degeneracy (grey shading). Upper right: the fiducial model with $T_{\rm min} = 10^4$ K and $T_{\rm ion} = 10^5$ K. Constraints on $\dot{\rho}_\star$ are used at $z > 4$. Lower left: a model with $T_{\rm min} = T_{\rm ion} = 10^4$ K. Constraints on Γ_{12} and $\dot{\rho}_\star$ are used at $z > 4$. Lower right: a model with $T_{\rm min} = 10^4$ K and $T_{\rm ion} = 10^5$ K, and $f_{\rm esc} \propto (1 + z)$. Constraints on Γ_{12} and $\dot{\rho}_\star$ are used at $z > 4$. In each case, three contours are shown corresponding to differences in χ^2 relative to the best-fitting model of $\Delta\chi^2 = \chi^2 - \chi^2_{\rm min} = 1$, 2.71 and 6.63. Projections of these contours on to the axes provide the 68.3, 90 and 99 per cent confidence intervals on individual parameter values. The large dots show parameters of model histories presented in Fig. 1.

conclusion regarding the value of escape fraction to the use of Γ as a constraint, we therefore investigate the constraints available when only the observations of $\dot{\rho}_\star$ are used in addition to $\tau_{\rm es}$. The constraints are shown in the upper-right panel of Fig. 2. In this case, the best-fitting model has the same parameter combination $(f_\star, f_{\rm esc}) = (0.105, 0.046)$, with a lower value of $\chi^2_{\rm min} = 0.3$. Thus, removing the Γ points loosens the constraints on $f_\star$ and $f_{\rm esc}$ but does not alter the best-fitting values. We find values of $0.072 \lesssim f_\star \lesssim 0.15$ and $0.022 \lesssim f_{\rm esc} \lesssim 0.12$ in this case.

In Fig. 3, we show the marginalized distribution of $f_{\rm esc}$. The line styles are consistent with those chosen for the corresponding contours of χ^2 in Fig. 2. In constructing the marginalized likelihoods we have assumed prior probability distributions for $f_\star$ and $f_{\rm esc}$ that are flat in the logarithm, i.e. $\mathrm{d}P_{\rm prior}/\mathrm{d}\log f_\star \propto 1$ and $\mathrm{d}P_{\rm prior}/\mathrm{d}\log f_{\rm esc} \propto 1$.

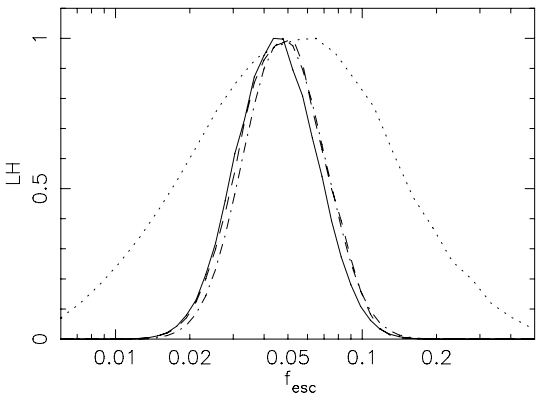

Figure 3. Constraints on the parameter $f_{\rm esc}$ corresponding to marginalization of the joint distributions in Fig. 2 (the line styles are the same for the joint and marginalized distributions in these figures). Solid line: the fiducial model with $T_{\rm min} = 10^4$ K and $T_{\rm ion} = 10^5$ K. Constraints on Γ_{12} and $\dot{\rho}_\star$ are used at $z > 4$. Dotted line: constraints on the fiducial model without the inclusion of Γ_{12}. Dashed line: a model with $T_{\rm min} = T_{\rm ion} = 10^4$ K. Constraints on Γ_{12} and $\dot{\rho}_\star$ are used at $z > 4$. Dot–dashed Line: a model with $T_{\rm min} = 10^4$ K and $T_{\rm ion} = 10^5$ K, and $f_{\rm esc} \propto (1 + z)$. Constraints on Γ_{12} and $\dot{\rho}_\star$ are used at $z > 4$.

5.3 Effect of radiative feedback on low-mass galaxies

There is some theoretical uncertainty surrounding the strength of radiation feedback on the formation of low-mass galaxies (Dijkstra et al. 2004; Mesinger & Dijkstra 2008). We therefore repeat our constraints on $f_\star$ and $f_{\rm esc}$ using a modification of the fiducial model with no radiative feedback, i.e. $T_{\rm min} = T_{\rm ion} = 10^4$ K. The constraints based on this model are shown in the lower-left panel of Fig. 2. The best-fitting modified model has the parameter combination $(f_\star, f_{\rm esc}) = (0.070, 0.046)$, with a value of $\chi^2_{\rm min} = 9.2$ (this model is therefore disfavoured by the data relative to the fiducial case). As reionization progresses, more gas is allowed to accrete into galaxies in this case than in the fiducial model. As a result, the star formation efficiency required to produce the observed star formation rate density is reduced. We find values of $0.05 \lesssim f_\star \lesssim 0.10$ and $0.03 \lesssim f_{\rm esc} \lesssim 0.07$ for this model. Thus, the details of the stellar mass accretion rate influence the inferred star

Downloaded from http://mnras.oxfordjournals.org/ by guest on February 28, 2013

formation efficiency, but only weakly affect the inferred escape fraction of ionizing photons.

Fig. 3 shows the corresponding marginalized distribution for escape fraction (dashed line). As noted above, the removal of radiative feedback from the model has little effect on the derived escape fraction distribution. On the other hand, the reionization history is quite different in this case. The dashed lines in Fig. 1 show the best-fitting model in this case $(f_\star,\ f_{\rm esc}) = (0.07,\ 0.046)$. The lower value of $f_\star$ means that reionization gets underway later. However, despite this reionization is finished earlier, with an associated rise in the ionizing background at higher redshifts in this case than in the fiducial model. This rapid rise occurs because reionization is assumed not to be self-limiting in this case and so is completed by low-mass galaxies.

5.4 Evolving escape fraction

Our modelling so far has assumed an escape fraction that is constant with redshift during reionization (i.e. at $z \gtrsim 6$), whereas there is some evidence from lower redshifts ($1 < z < 4$) that the escape fraction may evolve (Inoue et al. 2006; Razoumov & Sommer-Larsen 2006). To test the impact of this assumption on the value of $f_{\rm esc}$ we therefore consider a case where our fiducial model is modified so that $f_{\rm esc}(z) = f_{\rm esc}(1+z)/7$, and constrain the value of $f_{\rm esc}$ at $z = 6$. The results are shown in the lower-right panel of Fig. 2. In this case, we find values which are very similar to the fiducial case, $0.072 \lesssim f_\star \lesssim 0.15$ and $0.035 \lesssim f_{\rm esc} \lesssim 0.08$ for this model. The best-fitting model has the parameter combination $(f_\star,\ f_{\rm esc}) = (0.105,\ 0.050)$, with a value of $\chi^2_{\rm min} = 5.5$ (this model is therefore also disfavoured relative to the fiducial case).

Fig. 3 shows the corresponding marginalized distribution for escape fraction (dot–dashed line). The evolution of escape fraction is degenerate with evolution in the mass accretion rate of galaxies, and so, as in the previous example, has little effect on the derived escape fraction distribution. The dot–dashed lines in Fig. 1 show the best-fitting model in this case $(f_\star,\ f_{\rm esc}) = (0.105,\ 0.050)$. The reionization history is again quite different from the fiducial model. The larger value of $f_{\rm esc}$ towards high redshift results in an earlier reionization and a higher $\tau_{\rm es}$.

5.5 Uncertainty in the choice of IMF and metallicity

Both the number of ionizing photons produced per star and the star formation rate density inferred from the number of GRBs observed during the reionization era depend on the IMF assumed. In the fourth column of Table 1, we show the fraction of the star formation inferred assuming a Salpeter IMF that would have been derived in Kistler et al. (2009) if a different IMF had been used instead. Where a more top-heavy IMF is assumed, the star formation rate density implied by the observed GRBs is reduced by this factor relative to our fiducial model. Since a change in the assumed IMF leads to a change in the inferred star formation rate density, it also leads to a proportional change in the derived star formation efficiency. Thus, for each IMF listed the value of $\dot\rho_\star/\dot\rho_{\rm sal}$ represents the size of the systematic uncertainty in constraints on $f_\star$. On the other hand, a change in IMF also leads to a change in N_γ (see columns 5 and 6 of Table 1), and the escape fraction required to reproduce the observables of reionization is therefore proportional to $(\dot\rho_\star N_\gamma)^{-1}$. For a particular IMF, we can compute the quantity

$$f_{\rm IMF} \equiv \frac{N_\gamma}{N_{\rm sal}} \times \frac{\dot\rho_\star}{\dot\rho_{\rm sal}}, \qquad (7)$$

which gives the ratio of ionizing photons to GRBs, relative to the Salpeter IMF. The range in values of $f_{\rm IMF}$ provides an estimate of the systematic uncertainty in the derived escape fraction owing to the choice of IMF. In the final column of Table 1, we list the quantity $f_{\rm IMF}$ of the range of IMFs.

In each case, we find $f_{\rm IMF} \sim 1$ and so the net effect on the estimate of escape fraction caused by choosing a different IMF is quite modest. It is possible that the IMF is evolving with look-back time. In this case, by extension of the above arguments our estimate of the escape fraction would sustain only a small systematic uncertainty. Importantly, we find that for metal-enriched stellar populations, the choice of IMF contributes a systematic uncertainty on the derived escape fraction of only $\sim$0.1 dex.

Before continuing, we briefly discuss the contributions to equation (7). As already noted, the first ratio term arises because more massive stars are hotter and therefore emit a larger fraction of their energy at frequencies above the ionization threshold for hydrogen. Regarding the second term, we note that the relation between the GRB rate and the star formation rate density is calibrated at redshifts below $z \sim 4$ where they can each be separately determined (Kistler et al. 2009). Most of the star formation rate indicators (e.g. Hα) probe only massive stars, and hence a correction involving an IMF is required. However, what is important for the present analysis is the number of ionizing photons implied by the observed number of high-redshift GRBs, i.e. relating one quantity depending just on massive stars to another. With respect to this quantity, the dependencies on IMF mentioned tend to cancel, because a more top-heavy IMF leads to increases in both the GRB rate and the number of ionizing photons produced. We note here that within the context of studies of the star formation history, top-heavy can really be interpreted to mean bottom-light. This is because one measures the light (or the birth/death rate) from the massive stars and infers the contribution to stellar mass from lower masses. In other words, the analysis is normalized by the high-mass end of the IMF. This situation would be reversed if one were looking at the integrated stellar mass, which is dominated by low-mass stars.

Finally, we note that the assumed metallicity can have an effect on both the calibration of star formation rate density and on the value of N_γ computed for a particular IMF. Calibrations of star formation rate density are performed locally, and so refer to solar metallicity. On the other hand, we have assumed a metallicity of 1/20th solar in computing the reionization history, as may be more appropriate at high redshift. The Salpeter IMF with solar metallicity yields $N_\gamma = 3328$ ionizing photons per baryon, a factor of 1.4 times smaller than in our fiducial model. This metallicity uncertainty corresponds to an additional $\sim$0.1 dex uncertainty on $f_{\rm esc}$. It may be possible to remove this metallicity uncertainty in the determination of $f_{\rm esc}$ by noting that many star formation rate indicators (e.g. Hα) are proportional to the ionizing flux, so that the higher number of ionizing photons for low-metallicity stars is offset by a smaller inferred star formation rate. We have not pursued this in the current work. We conservatively estimate that accounting for the uncertainties in IMF and metallicity leads to $\sim$0.2 dex of systematic uncertainty in the determination of $f_{\rm esc}$ from our analysis.

5.6 Reionization by X-rays

Our analysis has thus far assumed that reionization is entirely due to high-mass stars. However, in addition to UV photons from the first galaxies and quasars, it has been suggested that a background of X-ray photons at very high redshift may be important (e.g. Ricotti & Ostriker 2004). Indeed, several authors have proposed

Downloaded from http://mnras.oxfordjournals.org/ by guest on February 28, 2013

an initial phase of preheating and partial ionization of the IGM by X-rays, resulting primarily from black hole accretion (e.g. Shull & van Steenberg 1985; Venkatesan, Giroux & Shull 2001; Ricotti & Ostriker 2004). An X-ray background could also have originated from X-ray binaries and supernova remnants. In difference to UV photons, X-rays ionize hydrogen both directly and through secondary ionizations by photoelectrons from ionized helium, with the latter dominating so that many hydrogen atoms can be ionized by a single X-ray photon. As reionization proceeds, however, the proportion of each X-rays energy that is deposited into the IGM as heat increases. In particular, for ionization fractions $\gtrsim$10 per cent, ionization by secondary electrons becomes inefficient (Ricotti & Ostriker 2004). As a result, X-ray ionization is self-regulating at the level of ∼10–20 per cent. Modelling the possible contribution of X-rays to reionization is beyond the scope of this paper. However, the self-regulation implies that neglect of X-rays would lead to an overestimation of $f_{\rm esc}$ by this factor at most, and we therefore estimate a systematic component of uncertainty owing to the unknown X-ray contribution to reionization of ∼0.05 dex.

5.7 Effect of dust

We note that dust has recently been shown to be an important consideration with respect to estimating the escape fraction (Yajima et al. 2009). Our approach implicitly takes the effects of dust into account, although it does not appear explicitly in our analysis for the following reasons. First, the rate of GRB detections is not affected by dust, while the effects of dust on estimates of the corresponding star formation rate are included in the calibration from lower redshift (Yüksel et al. 2008; Kistler et al. 2009). Secondly, our estimate of escape fraction is derived from the ratio of ionizing photons that enter the IGM and so ionize hydrogen to the number that are produced within galaxies (obtained from the star formation rate). The values of escape fraction obtained therefore include the effects of absorption by dust.

6 NUMERICAL CONSTRAINTS ON THE ESCAPE FRACTION

Our fiducial model constrains the escape fraction in the redshift range $4 < z < 8$ to have a value $\log f_{\rm esc} = -1.35 \pm 0.15$ (68 per cent). Of the systematic errors discussed, the largest arise due to uncertainty in the IMF and in the metallicity of the star-forming populations responsible for reionization. We estimate that each of these contributes ∼0.1 dex of systematic uncertainty. Thus, in summary of our analysis we find $\log f_{\rm esc} = (-1.35 \pm 0.15) \pm 0.2$.

6.1 Comparison to Lyα forest-derived constraints

As summarized in the Introduction, estimates of the escape fraction based on transmission in the Lyα forest yield a range of results (Inoue et al. 2006; Bolton & Haehnelt 2007; Srbinovsky & Wyithe 2008; Faucher-Giguère et al. 2008). Of these, most studies yield results of the order of 5–20 per cent in agreement with the results of this paper. However, Faucher-Giguère et al. (2008) find a lower value of ∼1 per cent, which is inconsistent with our findings where the Lyα forest constraints are included, and only barely consistent with our results where the Lyα forest is excluded from the analysis. Before concluding we present a short discussion of this discrepancy.

The simplest interpretation is that there is evolution in the escape fraction (Inoue et al. 2006). The analysis of Faucher-Giguère et al. (2008) was performed at $2 < z < 4$, while the results of Bolton & Haehnelt (2007) and Srbinovsky & Wyithe (2008) (as well as this paper) refer to redshifts close to or during reionization. However, in addition, the definition of escape fractions varies. For example, in this paper we refer to the escape fraction as the fraction of photons produced by stars that enter the IGM, whereas, for example, the definition of escape fraction used in Faucher-Giguère et al. (2008) takes the ratio of photons between 900 and 1500 Å (a definition more easily related to direct observations). The correction factors required to relate these definitions include the size of the Lyman break as well as dust attenuation of the UV continuum. These factors are opposite in effect but are both very uncertain.

There are also other important factors when modelling the Lyα forest. When converting from an observed absorption to an ionization rate, a temperature must be assumed for the IGM (this is the greatest source of uncertainty.). In order to derive an escape fraction, two additional ingredients are required. First, both a mean-free path and an SED for the ionizing sources must be assumed to convert from ionization rate to an ionizing emissivity [Faucher-Giguère et al. (2008) used a somewhat larger mean-free path than previous studies.]. Secondly, to go from an ionizing emissivity to an escape fraction, an estimate of star formation rate density is needed. In Faucher-Giguère et al. (2008), a large value was used for the star formation rate, with the luminosity function extrapolated to low luminosities to correct for the incompleteness from missing faint galaxies. This could lead to an underestimation of the escape fraction if the number of faint galaxies were overestimated. A similar problem appears in the estimates of the Lyα forest from high redshift. For example Bolton & Haehnelt (2007) find a large value of ∼20 per cent. This could possibly be due to an underestimate of the star formation rate density due to the faint galaxies missing from surveys for high-redshift galaxies (Kistler et al. 2009).

Our study still contains uncertainties related to the Lyα forest, namely the mean-free path and the assumed temperature, at least in cases where the ionization rate is included as a constraint. However, we have mitigated several of the other major uncertainties. In particular, the use of GRBs as a proxy for star formation provides a direct average over the whole population of galaxies without corrections for unseen faint galaxies. Moreover, the inclusion of the optical depth to electron scattering of CMB photons provides a direct (though not unique) probe of the reionization history. The resulting comparison between ionizing photons produced and the number of ionizations required at a particular redshift does not require the intermediate step of a mean-free path, and so gives a less model-dependent handle on the escape fraction than is available from the Lyα forest alone.

7 SUMMARY

The fraction of ionizing photons that escape their host galaxy and so are able to ionize hydrogen in the IGM is a critical parameter in studies of the reionization era and early galaxy formation. Indeed, the amount of star formation required to reionize the Universe is inversely proportional to the escape fraction. Determination of the expected value for the escape fraction is problematic for individual galaxies. Observationally, very deep spectra must be obtained to overcome absorption in the IGM and detect photons that escape the host galaxy at energies beyond the Ly limit. Theoretical calculation of escape fraction is difficult owing to the large dynamic range and complex gas and star formation physics that must be modelled to resolve the clumpy ISM.

Many studies of the reionization history have compared theoretical models to the electron scattering optical depth of CMB

Downloaded from http://mnras.oxfordjournals.org/ by guest on February 28, 2013

photons, and the ionization rate from the Lyα forest at the end of the overlap era. These studies are subject to degeneracies between the escape fraction of ionizing photons and the efficiency with which high-redshift galaxies turn mass into stars (e.g. Wyithe & Loeb 2003; Haiman & Holder 2003; Cen 2003; Choudhury & Ferrara 2005; Shull & Venkatesan 2008). While upper limits have previously been obtained for surveys of high-redshift star-forming galaxies (Bouwens et al. 2008), the recent determination of the star formation rate density during the reionization era from the most distant GRBs discovered provides the first method for directly measuring the star formation rate density during the reionization era. With respect to calculating the escape fraction, this method has the advantages over estimates of star formation rate from the galaxy luminosity function that it directly observes the total star formation rate (i.e. no correction for a galaxy flux limit), and is well calibrated at lower redshift (Kistler et al. 2009).

In this paper, we have used this first determination of the star formation rate density at $z > 6$ to break the degeneracy between star formation efficiency and escape fraction. Our analysis employed a semi-analytic model for reionization that we confronted with three complementary sets of observations: (i) the electron scattering optical depth of CMB photons; (ii) the ionization rate from the Lyα forest at the end of the overlap era and (iii) the star formation rate density out to $z = 8.5$. By constraining the model parameters with these observations we show that the escape fraction of ionizing photons from high-redshift galaxies is $f_{\rm esc} \sim 5$ per cent. For our fiducial model we find $\log f_{\rm esc} = -1.35 \pm 0.15$. This relatively small value of escape fraction follows from the slow evolution in the star formation rate density at $z \gtrsim 4$ implied by the number counts of high-redshift GRBs.

Importantly, this value is stable against a range of systematic uncertainties in the modelling, including the implementation of radiative feedback and the choice of IMF. In agreement with previous studies, we find that the mass assembly history of galaxies was important for the reionization history, and impacts on the inferred value of star formation efficiency. However, the value of escape fraction inferred is not sensitive to the details of the mass assembly. We also investigated an evolving escape fraction, finding that this did not strongly influence the value of escape fraction inferred for galaxies at $z = 6$. Our modelling does make the assumption that UV photons produced by stars dominate the reionization process. A possible contribution of X-rays to reionization (Ricotti & Ostriker 2004) complicates this interpretation, and implies that our escape fraction could be overestimated by a factor up to 1.1–1.2. Both the number of ionizing photons and the number of GRBs per unit star formation are sensitive to the IMF. The dependencies on IMF tend to cancel in our analysis; however we considered a range of possibilities. We estimate an uncertainty of $\sim$0.1 dex in $f_{\rm esc}$ owing to the unknown shape of the IMF, and another $\sim$0.1 dex owing to the unknown metallicity of the galaxies responsible for reionization. Including these uncertainties, we express our estimate of escape fraction as $\log f_{\rm esc} = (-1.35 \pm 0.15) \pm 0.2$. Our analysis assumed that the escape fraction is independent of galaxy mass. Previous work has suggested that escape fraction may be mass dependent (Gnedin et al. 2008; Wise & Cen 2009). In this scenario, our escape fraction should be considered as a stellar mass weighted average over star-forming galaxies.

Our simple semi-analytic model is able to provide a statistically acceptable fit to the available observations under a range of assumptions. This implies that models of the reionization history are underconstrained [although more variables could potentially be used as constraints (Choudhury & Ferrara 2005, 2006)]. In the near future, 21-cm observations of neutral IGM during the reionization era will provide a powerful new probe. Lidz et al. (2008) have shown that the first generation of low-frequency telescopes will be able to measure the neutral fraction accurately during epochs when the universe is $\sim$50 per cent ionized. The example reionization histories presented in this and other papers illustrate that this will provide important discriminates among possible reionization histories. Such measurements, in combination with the star formation rate density, will allow for the evolution of escape fraction to be measured in addition to its value.

ACKNOWLEDGMENTS

This work was supported in part by the Australian Research Council (JSBW and AMH). MDK and JFB were supported by NSF CAREER Grant PHY-0547102 (to JFB) and HY by DOE Grant DE-FG02-91ER40626.

REFERENCES

Baldry I. K., Glazebrook K., 2003, ApJ, 593, 258
Barkana R., Loeb A., 2001, ApJS, 349, 125
Bland-Hawthorn J., Maloney P. R., 1999, ApJ, 510, L33
Bolton J. S., Haehnelt M. G., 2007, MNRAS, 382, 235
Bouwens R. J., Illingworth G. D., Franx M., Ford H., 2008, ApJ, 686, 230
Cen R., 2003, ApJ, 591, L5
Chen H.-W., Prochaska J. X., Gnedin N. Y., 2007, ApJ, 667, L125
Choudhury T. R., Ferrara A., 2005, MNRAS, 361, 577
Choudhury T. R., Ferrara A., 2006, MNRAS, 371, L55
Cowie L. L., Barger A. J., Trouille L., 2009, ApJ, 692, 1476
Deharveng J.-M., Buat V., Le Brun V., Milliard B., Kunth D., Shull J. M., Gry C., 2001, A&A, 375, 805
Dijkstra M., Haiman Z., Rees M. J., Weinberg D. H., 2004, ApJ, 601, 666
Efstathiou G., 1992, MNRAS, 256, 43
Fan X., Narayanan V. K., Strauss M. A., White R. L., Becker R. H., Pentericci L., Rix H. W., 2002, AJ, 123, 1247
Fan X. et al., 2006, AJ, 132, 117
Faucher-Giguère C.-A., Lidz A., Hernquist L., Zaldarriaga M., 2008, ApJ, 688, 85
Fernández-Soto A., Lanzetta K. M., Chen H.-W., 2003, MNRAS, 342, 1215
Fruchter A. S. et al., 2006, Nat, 441, 463
Fujita A., Martin C. L., Mac Low M.-M., Abel T., 2003, ApJ, 599, 50
Fynbo J. P. U. et al., 2009, preprint (arXiv:0907.3449)
Gehrels N., 1986, ApJ, 303, 336
Gnedin N. Y., Kravtsov A. V., Chen H.-W., 2008, ApJ, 672, 765
Haiman Z., Holder G. P., 2003, ApJ, 595, 1
Hopkins A. M., Beacom J. F., 2006, ApJ, 651, 142
Inoue A. K., Iwata I., Deharveng J.-M., 2006, MNRAS, 371, L1
Iwata I. et al., 2009, ApJ, 692, 1287
Kistler M. D., Yüksel H., Beacom J. F., Stanek K. Z., 2008, ApJ, 673, L119
Kistler M. D., Yuksel H., Beacom J. F., Hopkins A. M., Wyithe J. S. B., 2009, ApJ, 705, 104
Komatsu E. et al., 2009, ApJS, 180, 330
Leitherer C., Ferguson H. C., Heckman T. M., Lowenthal J. D., 1995, ApJ, 454, L19
Leitherer C. et al., 1999, ApJS, 123, 3
Lidz A., Zahn O., McQuinn M., Zaldarriaga M., Hernquist L., 2008, ApJ, 680, 962
Lien A., Fields B. D., 2009, J. Cosmol. Astro-Part. Phys., 1, 47
Madau P., Haardt F., Rees M. J., 1999, ApJ, 514, 648
Mesinger A., Dijkstra M., 2008, MNRAS, 390, 1071
Miralda-Escudé J., Haehnelt M., Rees M. J., 2000, ApJ, 530, 1
Oh S. P., Furlanetto S. R., 2005, ApJ, 620, L9
Press W. H., Schechter P., 1974, ApJ, 187, 425
Prochaska J. X., Herbert-Fort S., Wolfe A. M., 2005, ApJ, 635, 123
Razoumov A. O., Sommer-Larsen J., 2006, ApJ, 651, L89

Downloaded from http://mnras.oxfordjournals.org/ by guest on February 28, 2013

Ricotti M., Ostriker J. P., 2004, MNRAS, 352, 547
Salvaterra R. et al., 2009, preprint (astro-ph/0906.1578)
Shapley A. E., Steidel C. C., Pettini M., Adelberger K. L., Erb D. K., 2006, ApJ, 651, 688
Shull J. M., van Steenberg M. E., 1985, ApJ, 298, 268
Shull J. M., Venkatesan A., 2008, ApJ, 685, 1
Siana B. et al., 2007, ApJ, 668, 62
Srbinovsky J. A., Wyithe J. S. B., 2007, MNRAS, 374, 627
Srbinovsky J., Wyithe S., 2008, preprint (astro-ph/0807.4782)
Stanek K. Z. et al., 2006, Acta Astronomica, 56, 333
Steidel C. C., Pettini M., Adelberger K. L., 2001, ApJ, 546, 665
Storrie-Lombardi L. J., McMahon R. G., Irwin M. J., Hazard C., 1994, ApJ, 427, L13
Tanvir N. R. et al., 2009, preprint (astro-ph/0906.1577)
Thoul A. A., Weinberg D. H., 1996, ApJ, 465, 608
Venkatesan A., Giroux M. L., Shull J. M., 2001, ApJ, 563, 1
Wise J. H., Cen R., 2009, ApJ, 693, 984
Wood K., Loeb A., 2000, ApJ, 545, 86
Wyithe J. S. B., Loeb A., 2003, ApJ, 586, 693
Wyithe J. S. B., Bolton J. S., Haehnelt M. G., 2008, MNRAS, 383, 691
Yajima H., Umemura M., Mori M., Nakamoto T., 2009, MNRAS, 398, 715
Yüksel H., Kistler M. D., Beacom J. F., Hopkins A. M., 2008, ApJ, 683, L5

This paper has been typeset from a TEX/LATEX file prepared by the author.

Downloaded from http://mnras.oxfordjournals.org/ by guest on February 28, 2013